Correlation of the plasmon-enhanced photoconductance and photovoltaic properties of core-shell Au@TiO_2 network

Yiqun Yang, Judy Wu, and Jun Li'

Citation: Appl. Phys. Lett. **109**, 091604 (2016); doi: 10.1063/1.4961884

View online: http://dx.doi.org/10.1063/1.4961884

View Table of Contents: http://aip.scitation.org/toc/apl/109/9

Published by the American Institute of Physics

Correlation of the plasmon-enhanced photoconductance and photovoltaic properties of core-shell Au@TiO_2 network

Yiqun Yang,[1] Judy Wu,[2] and Jun Li[1,3,a)]
[1]*Department of Chemistry, Kansas State University, Manhattan, Kansas 66506, USA*
[2]*Department of Physics and Astronomy, University of Kansas, Lawrence, Kansas 66045, USA*
[3]*College of Chemistry and Chemical Engineering, Hubei Normal University, Huangshi, Hubei 435002, People's Republic of China*

(Received 20 July 2016; accepted 17 August 2016; published online 30 August 2016)

This study reveals the contribution of hot electrons from the excited plasmonic nanoparticles in dye sensitized solar cells (DSSCs) by correlating the photoconductance of a core-shell Au@TiO_2 network on a micro-gap electrode and the photovolatic properties of this material as photoanodes in DSSCs. The distinct wavelength dependence of these two devices reveals that the plasmon-excited hot electrons can easily overcome the Schottky barrier at Au/TiO_2 interface in the whole visible wavelength range and transfer from Au nanoparticles into the TiO_2 network. The enhanced charge carrier density leads to higher photoconductance and facilitates more efficient charge separation and photoelectron collection in the DSSCs. *Published by AIP Publishing.*
[http://dx.doi.org/10.1063/1.4961884]

Noble metal nanoparticles (NPs) have been widely applied for light engineering in photoactive devices, such as solar cells, light-emitting diodes, and photocatalysis systems, to enhance the device performance.[1] Extra photon energy can be absorbed and concentrated by the surface plasmonic resonance (SPR) arising from the collective oscillation of free electrons in metal NPs under visible irradiation.[2] Plasmonically enhanced dye sensitized solar cells (DSSCs) is a good example. Photoconversion in traditional DSSCs is achieved by a wide-bandgap semiconductive TiO_2 layer sensitized with organic dye molecules that have strong absorptivity of visible light.[3] Enhanced photocurrents were observed in the DSSCs consisting of small amounts of noble metal plasmonic NPs blended in the active anode materials. Generally, the plasmonic NPs can enhance dye excitation through either an intensified near-field or enhanced light-scattering.[4] To suppress these conductive metal NPs acting as electron drains, core-shell structure was adopted by coating noble metal NPs with a compact thin layer of non-conductive metal oxide that effectively prevents unwanted electron-hole recombination.[5] Particularly, semiconductive TiO_2 was proposed as a better shell material than other insulative oxides (such as SiO_2) due to its higher capability to extract electrons from the excited dyes and compatibility with the surrounding TiO_2 matrix in the DSSC anode.[6] Recent studies proposed that the metal/TiO_2 interface in the TiO_2-encapsulated metal NPs, i.e., metal@TiO_2, may form an interfacial energy barrier (so-called Schottky barrier) to prevent normal electron flowing across, but hot electrons from plasmon-excited metal cores could easily overcome this energy barrier and be injected into the TiO_2 conduction band (CB), resulting in a new mechanism for plasmon enhancement in the DSSCs.[7]

In general, the injected hot electrons are considered either being converted into photocurrent or functioning as charge carriers in the semiconductor matrix.[8] The photocurrent generated by direct hot electron transfer across the Schottky barrier has been collected and utilized for photodetection and photovoltaics based on the well-designed devices with a complete circuit allowing refilling electrons back to the metal.[9] However, for the metal@TiO_2 NPs embedded in the mesoporous TiO_2 film in the DSSCs, the sustainability of the photocurrent generation from hot electron injection is under debate considering that the metal core is unaccessible to the electron donors or the external circuit, which are needed for charge regeneration. On the other hand, the initially injected hot electrons may be converted into steady-state charge carriers and sufficiently raise the conductivity of the mesoporous TiO_2 frame, as has been indirectly demonstrated by the obseravations of photoconductance enhancement in the metal coupled semiconductors.[10] In addition, a recent study by Cushing *et al.* have reported that metal@TiO_2 and metal@SiO_2@TiO_2 NPs can also enhance the DSSCs by exciting surrounding TiO_2 matrix and dye molecules with near-field based plasmon-induced resonance energy transfer (PIRET) beside hot electron injection.[11] We have also confirmed such effects in the DSSCs sensitized with natural light harvesting complex II.[12] In most DSSC operations, these three effects are mixed. It is necessary to design some model systems to elucidate the contributions of these distinctive effects in order to understand the complex mechanisms of the plasmon-enhanced DSSCs.

Here, we propose a strategy to sort out the contributions of hot electron injection by comparing the characteristics of two model devices, i.e., micro-gap electrodes and DSSCs. A core-shell material consisting of isolated Au NPs embedded at the nodes of a nanostructured TiO_2 network, i.e., Au@TiO_2 network, was used as the bridging material in the micro-gap between two Au electrodes and as the mesoporous film on a DSSC anode, respectively. This study allows isolating the plasmonic effects on electron transport across the network structure[13] and linking it with the enhanced photocurrents in DSSCs. These two devices present distinct wavelength dependences, revealing their different dominant

a)E-mail: junli@ksu.edu

plasmonic mechanisms. The correlation of the plasmonically enhanced photoconductance and photovoltaic properties unambiguously reveals that the major role of hot electrons in the enhanced DSSCs is to enhance the electrical conductivity of the TiO_2 network.

Synthesis of Au@TiO_2 network was defined in two steps. In the first step, a TiO_2 layer of ~8 nm was coated outside the surface of 20 nm Au NPs (Fig. 1(b)). The growth of TiO_2 shell started with a heterogeneous nucleation process requiring to critically control the low concentration of TiO_2 oligomers in solution, which competes with the formation of isolated TiO_2 NPs via homogeneous nucleation.[14] In the second step, the homogeneous reaction among the TiO_2 oligomers dominated after adding more precursors, and the core-shell Au/TiO_2 NPs formed in the first step were crosslinked into the amorphous TiO_2 network as shown in Fig. 1(c) which consists of ~7 wt. % of Au NPs. More details on materials preparation and characterization are described in the experimental section in the supplementary material. The SEM image in Fig. 1(d) confirmed that the network structure retained in the sample after drop-casting on the micro-gap electrode and subsequent thermal annealing process (illustrated in the inset of Fig. 1(d)).

The plasmonic band of Au@TiO_2 NPs overlaps with the whole absorption peak of N719 dye (see supplementary material, Fig. S1(a)), which is ideal for the near-field plasmonic enhancement, and it does not show any obvious shift after forming the Au@TiO_2 network (data not shown). In order to confirm that the TiO_2 shell fully covers the Au NPs, the Au@TiO_2 network was drop-casted on a transparent glass substrate coated with a layer of fluorine-doped tin oxide (FTO) and annealed at 350 °C in the air for 1 h. The prepared sample was then immersed in iodide/triiodide (I^-/I_3^-) electrolyte overnight. The absorption spectra after annealing and electrolyte treatment are presented in Fig. S1(b) of the supplementary material, which display negligible difference compared with the initial spectrum, demonstrating that the intact TiO_2 shell on the Au NPs is able to protect the Au NPs from both heat damage and iodide corrosion during the device fabrication and testing.

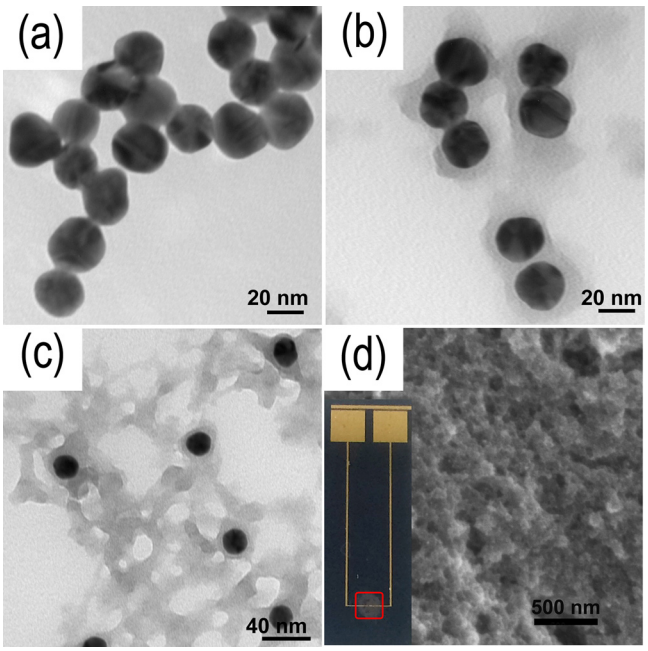

FIG. 1. TEM images of (a) bare gold nanoparticles, (b) Au@TiO_2 core-shell nanoparticles, and (c) Au@TiO_2 network. (d) SEM image of Au@TiO_2 network deposited on the micro-gap electrode after annealing. Inset: the photograph of micro-gap electrode with the Au@TiO_2 network material drop casted in the region of red box to cover the micro-gap.

To investigate the photoconductance, the I–V curves of the Au/TiO_2 network casted on the micro-gap electrode were recorded under dark and illuminated conditions. The annealed Au/TiO_2 network exhibited bigger increase in photoconductance as represented by the larger slope in the I–V curve under illumination in Fig. S2(b) in the supplementary material, which can be ascribed to the improved anatase crystallinity of TiO_2, as revealed by the Raman spectroscopy showing the characteristic bands of anatase phase at ~143, 197, 396, 516, and 639 cm^{-1} after thermal annealing (see Fig. S2(a) in the supplementary material). In contrast, under the dark condition, the annealed sample presents slightly smaller current than the un-annealed one. This could be due to the possibility of less oxygen vacancies in thermal annealed TiO_2 (as electron donors).[15,16]

As illustrated in Fig. 2(a), under 1 sun illumination, the slope of the I–V curve measured with the Au@TiO_2 network is much larger than that of the bare TiO_2 network, which is further raised after N719 dye sensitization on the exterior TiO_2 surface. The photoconductance (G) versus the bias voltage calculated from the first derivative of the I–V curve is shown in Fig. S3, which indicates higher photoconductance at high voltage bias (and electric field strength). But the trend of the change after incorporating bare and N719-derivatized Au/TiO_2 NPs is consistent over the whole voltage range. Fig. 2(b) shows synchronous responses of the photocurrent to 1 sun illumination at a medium bias of 0.2 V. All photocurrents are highly reproducible as the illumination is turned on and off for four cycles. The response is very

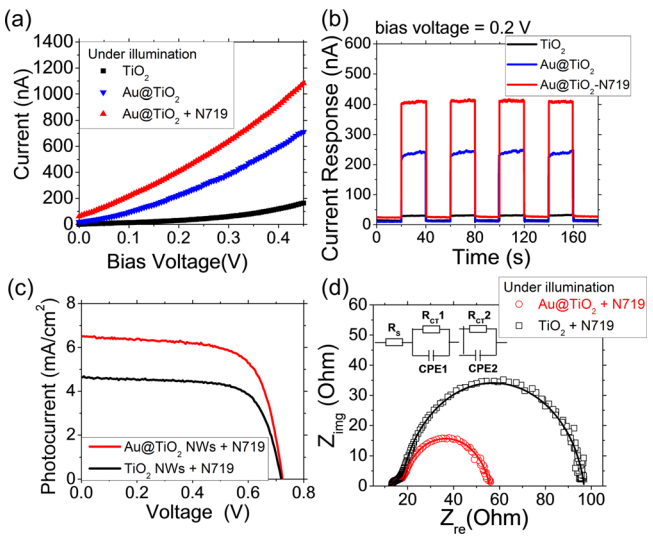

FIG. 2. (a) I–V curves measured with the micro-gap electrodes deposited with a bare TiO_2 network (black solid square), bare Au@TiO_2 network (blue solid down triangle), and Au@TiO_2 network sensitized with N719 (red solid up triangle) under 1 sun illumination. (b) Current responses at 0.2 V bias as the 1 sun illumination is switched on and off, respectively. All samples were annealed at 350 °C before dye sensitization and measurements. (c) I–V curves and (d) AC impedance spectra under 1 sun illumination of the DSSCs based on pure TiO_2 network (black curves) and Au@TiO_2 network (red curves), respectively. The impedance data are fitted with the equivalent circuit shown in the inset of panel (d).

fast, beyond the temporal resolution of the instrument (~40 ms) that is mainly defined by the shutter speed. The magnitudes of the photocurrent correlate well with the trend of the I–V curves in Fig. 2(a). These results concluded that the photoconductivity of the Au@TiO_2 network was enhanced (by 6.7 folds with respect to TiO_2 only) due to the incorporation of Au NPs, and it was further improved with dye sensitization (by additional 5.5 folds).

It is noted that both Au NPs and N719 dye help to harvest the solar photons in the visible range while the TiO_2 alone only absorbs UV light. The strong plasmonic excitation of Au NPs would generate significant amount of hot electrons which can overcome the ~0.9 eV Schottky barrier to transfer from Au NPs into TiO_2 shell. The injected hot electrons act as charge carriers and thus increase the photoconductivity of the TiO_2 network. With additional N719 dye sensitization, because the energy level of the lowest unoccupied molecular orbital (LUMO) of N719 (−3.85 eV) locates 0.55 eV higher than the edge of the CB of TiO_2 (−4.4 eV), the excited electrons can easily transfer from the dye to the TiO_2 network. This process could be enhanced by the energy transfer from plasmonic Au NPs to N719 dye passing through the thin TiO_2 shell, i.e., the near-field associated PIRET, since the plasmonic band of the incorporated Au NPs matches well with the absorption band of N719 (as shown in Fig. S1(a) in the supplementary material). This would further raise the charge carrier density in the TiO_2 network and thus make it even more conductive. Notably, the lack of spectral overlap of the Au NPs with the TiO_2 minimizes the PIRET between Au NPs and TiO_2 shell. Therefore, the enhanced photoconductivity of the non-sensitized Au/TiO_2 network must be dominated by hot electron injection, with more convincing evidence shown in the below paragraph.

The dark currents at the similar voltage bias in each corresponding samples (shown in Fig. S4 in the supplementary material) are about 20 times smaller than those obtained under 1 sun illumination, indicating a poor intrinsic conductivity of the TiO_2 network. It is noted that the Au@TiO_2 network shows slightly smaller dark current than the pure TiO_2 network. This may be due to the larger electron scattering and blocking of the carrier pathway by redistributed electron density at the Au/TiO_2 interface due to the Schottky barrier formation.[17] However, higher dark current was observed after dye sensitization, different from the previous studies on single TiO_2-coated carbon nanofibers.[16] Since the measurements were carried out in atmosphere, oxygen molecules as electron scavengers may "quench" the conduction electrons.[18] Dye molecules adsorbed on TiO_2 might suppress this carrier "quenching" via blocking the oxygen adsorption and thereby improve the intrinsic conductivity of the TiO_2 network.

The above discussed Au@TiO_2 network was prepared into a ~3 μm thick film on FTO-coated glass and used as an anode material in the DSSC for the purpose of correlating the enhanced photoconductivity with its photovoltaic performance. A pure TiO_2 network without the Au NPs was used as the control. The I–V curves and AC impedance spectra measured from these two types of DSSCs are plotted in Figs. 2(c) and 2(d). Obviously, much larger photocurrents were generated in the DSSC with the Au@TiO_2 network, which is mainly attributed to the aforementioned plasmonic near-field stimulated dye excitation, i.e., PIRET. The short-circuit current (J_{SC}) was increased to 6.54 mA/cm^2 with the Au@TiO_2 network compared to 4.64 mA/cm^2 with the pure TiO_2 network. The open circuit voltage (V_{OC}) was nearly the same for both DSSCs, implying that the core-shell structure was effective in suppressing the electron-hole recombination in the Au NPs. In addition, the series resistance calculated from the inverse of the slope of the I–V curve around V_{OC} was found to be reduced from 15 Ω to 11 Ω in presence of Au NPs. The AC impedance spectra under illumination exhibited much smaller charge transfer resistance after incorporating Au NPs, giving a $R_{CT,2}$ value of 38 Ω vs. 79 Ω, as reflected by the smaller semicircle at the low frequency range in the DSSC made of the Au@TiO_2 network. These data correlate well with the higher photoconductivity shown in Figs. 2(a) and 2(b), which conclusively prove that the higher charge carrier density and thus higher conductance are generated in the Au@TiO_2 network.

In order to understand the mechanisms of the above observation, the wavelength dependence of the photoconductance on the micro-gap electrode (under 0.2 V bias) was compared with the incident photon-to-current efficiency (IPCE) measurement of corresponding DSSCs (under short circuit). The IPCE was calculated with the equation,

$$\mathrm{IPCE}\% = 100\% \times (1240 \times J_{SC})/(\lambda \times P_{in}), \qquad (1)$$

where J_{SC} is the short circuit current and P_{in} is the power of incident photons at each wavelength. For a direct comparison, the wavelength dependence of the photoconductance was represented as the photocurrent divided by the number of incident photons at corresponding wavelengths using the similar equation, by replacing J_{SC} with the current measured under 0.2 V bias. The contribution of dark current is ignored since it is more than 100 times smaller than the current under illumination. The trend of the normalized photoconductance at all wavelengths in Fig. 3(a) correlates well with the illuminated I–V curves in Fig. 2(a), implying the large enhancement to the photoconductance by Au NPs embedded in the TiO_2 network. Interestingly, the enhancement appeared in a much broader range than the Au NP's SPR band, covering the full visible range from 400 to 800 nm. The enhanced current (by a factor of ~6) is almost constant over this wavelength range except a small dip around 600 nm. The photocurrent is further increased by another factor of ~10 after N719 dye sensitization, indicating the strong coupling between N719 dye and the plasmonic Au NPs.

In contrast, the IPCE curve of the DSSC made of the pure TiO_2 network shows a well-defined single peak in the visible range, whose peak wavelength at ~515 nm and the peak shape reflect the absorption spectrum of N719 dye. The IPCE value below 400 nm wavelength approximately monotonically decreases with the wavelength since the illumination is applied from the back side and the photons at shorter wavelength are absorbed by the glass substrate and FTO coating, as we demonstrated in an earlier study.[19] After incorporating Au NPs, the shape of the IPCE peak remains the same but the peak IPCE value is increased by ~41%. Notably, the long flat tails at longer wavelengths (600–800 nm) in Fig. 3(a) do not

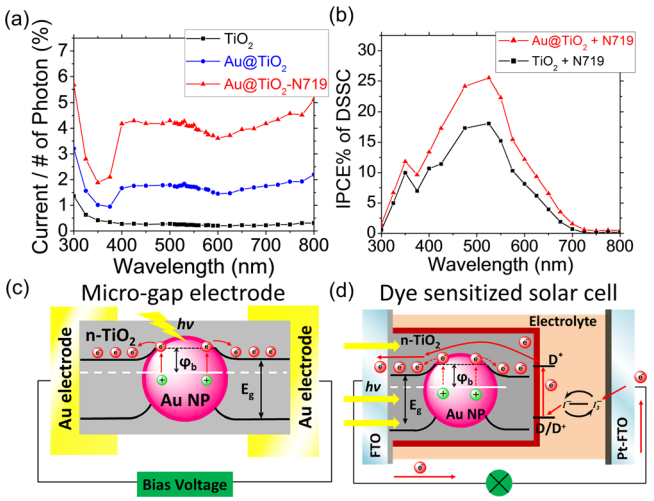

FIG. 3. (a) The wavelength dependence of photoconductance relative to the number of incident photons (in arbitrary unit) measured under 0.2 V bias on the micro-gap electrode after normalized to the number of incident photons. (b) The incident photon-to-current efficiency (IPCE%) of the DSSCs based on the pure TiO_2 network and $Au@TiO_2$ network, respectively. (c) and (d) The schematic of the potential mechanisms of the plasmonic effects in the $Au@TiO_2$ network on the micro-gap electrode and in the DSSC, respectively.

show in the IPCE curves of the corresponding DSSCs (Fig. 3(b)), but they are of great interests toward utilization of lower energy photons. These two types of devices are clearly based on different mechanisms.

The potential mechanisms of the plasmonic enhancement in photoconductance and the photovoltaics are schematically depicted in Figs. 3(c) and 3(d). As discussed previously, a Schottky barrier formed at the Au/TiO_2 interface would hinder the interfacial electron transfer in dark conditions. The barrier height (φ_b) is determined by the band structure of TiO_2 and the work function of gold, which is only ~0.9 eV (i.e., ~1378 nm in photon wavelength). As a result, not only the photons in the plasmonic band of the Au NPs but also all those in the full illumination range from 400 nm to 800 nm are energetic enough to generate hot electrons in the Au NPs that can be injected into the TiO_2 network. Thus, the charge carrier density in the semiconductive TiO_2 network is increased. In other words, the injected hot electrons act as the mobile charge carriers and are able to deliver larger currents under the same bias voltage. This mechanism nicely explains the I–V characteristics of the micro-gap experiments and the equally effective photoconductance enhancement by photons in the longer wavelength region. The charge carrier density likely reaches the saturation level even with the weak light absorbance of Au NPs at ~800 nm wavelength, thus forming a flat plateau.

The photovoltaic behavior of the DSSCs, however, is dominated by the charge separation at the dye/TiO_2 interface. The steady-state photocurrent requires electrons being continuously injected from the dye molecules into TiO_2 and the oxidized dye being quickly regenerated by reduction with I^-/I_3^- electrolyte. In the DSSC made of the $Au@TiO_2$ network, considering that the Au NPs embedded within the TiO_2 shell are not accessible by the regenerating agents, the plasmon-generated hot electrons from Au NPs to TiO_2 cannot be the source of continuous steady-state photocurrent. However, they are sufficient to raise the charge carrier density in TiO_2 and reduce the series resistance and charge transfer resistance in the corresponding DSSCs. This effect amplifies the characteristic features of the DSSC's IPCE curves which are determined by the charge separation initiated by photon absorption spectrum of the dye molecules. The correlation of the photovoltaic and photoconductance measurements clearly reveals the two distinct effects of plasmonic NPs which are entangled in normal plasmonic DSSCs.

In summary, the correlation between the enhanced photoconductivity and the photovoltaic performance of the as-synthesized core-shell $Au@TiO_2$ network deposited on the micro-gap electrodes and the photoanode of DSSCs facilitates discriminating contribution of the hot electron injection from that of the enhanced near-field effects. Hot electrons excited from the Au NPs are converted into major charge carriers in the TiO_2 network. The interfacial electron transfer across the Au/TiO_2 Schottky barrier (~0.9 eV) can be easily realized under illumination over the whole visible range, allowing extending the enhancement effect to the light in the near-infrared region where the photon energies are distinctively below the semiconductor band gap, Au SPR, and dye absorption band. This study may inspire future optoelectronic devices to make better use of hot electrons and the associated interfacial electron transfer for an outstanding performance.

See supplementary materials for experimental section, absorption spectra of Au/TiO_2 NPs in solution and on FTO glass subjected to annealing and I^-/I_3^- electrolyte treatment, Raman spectroscopy, and I–V characterization of unannealed and annealed samples.

This work was supported by the NSF EPSCoR Award No. EPS-0903806 (including the matching support from the State of Kansas through Kansas Technology Enterprise Corporation and a supplemental grant to J.L.), a NASA Grant No. NNX13AD42A and the matching fund provided by the State of Kansas. J.W. also acknowledges the support from NSF-DMR-1508494 and ARO-W911NF-16-1-0029. We acknowledge the help of Steven A. Klankowski in taking SEM images.

The authors declare no competing financial interest.

[1]H. A. Atwater and A. Polman, Nat. Mater. **9**, 205 (2010); A. Polman, Science **322**, 868 (2008); X. Gu, T. Qiu, W. Zhang, and P. K. Chu, Nanoscale Res. Lett. **6**, 199 (2011); X. Zhang, Y. L. Chen, R. S. Liu, and D. P. Tsai, Rep. Prog. Phys. **76**, 046401 (2013).
[2]K. L. Kelly, E. Coronado, L. L. Zhao, and G. C. Schatz, J. Phys. Chem. B **107**, 668 (2003).
[3]B. O'Regan and M. Grätzel, Nature **353**, 737 (1991).
[4]N. C. Jeong, C. Prasittichai, and J. T. Hupp, Langmuir **27**, 14609 (2011); W. Hou, P. Pavaskar, Z. Liu, J. Theiss, M. Aykol, and S. B. Cronin, Energy Environ. Sci. **4**, 4650 (2011); B. Ding, B. J. Lee, M. J. Yang, H. S. Jung, and J. K. Lee, Adv. Energy Mater. **1**, 415 (2011); S.-J. Lin, K.-C. Lee, J.-L. Wu, and J.-Y. Wu, Sol. Energy **86**, 2600 (2012).
[5]M. D. Brown, T. Suteewong, R. S. S. Kumar, V. D'Innocenzo, A. Petrozza, M. M. Lee, U. Wiesner, and H. J. Snaith, Nano Lett. **11**, 438 (2011); M. K. Gangishetty, K. E. Lee, R. W. J. Scott, and T. L. Kelly, ACS Appl. Mater. Interfaces **5**, 11044 (2013).
[6]J. Qi, X. Dang, P. T. Hammond, and A. M. Belcher, ACS Nano **5**, 7108 (2011); S. W. Sheehan, H. Noh, G. W. Brudvig, H. Cao, and C. A. Schmuttenmaer, J. Phys. Chem. C **117**, 927 (2013).

[7]Y. H. Jang, Y. J. Jang, S. T. Kochuveedu, M. Byun, Z. Lin, and D. H. Kim, Nanoscale **6**, 1823 (2014).
[8]C. Clavero, Nat. Photonics **8**, 95 (2014).
[9]M. W. Knight, H. Sobhani, P. Nordlander, and N. J. Halas, Science **332**, 702 (2011); E. W. McFarland and J. Tang, Nature **421**, 616 (2003); Y. Tian and T. Tatsuma, J. Am. Chem. Soc. **127**, 7632 (2005); Z. H. Chen, Y. B. Tang, C. P. Liu, Y. H. Leung, G. D. Yuan, L. M. Chen, Y. Q. Wang, I. Bello, J. A. Zapien, W. J. Zhang, C. S. Lee, and S. T. Lee, J. Phys. Chem. C **113**, 13433 (2009).
[10]M.-S. Son, J.-E. Im, K.-K. Wang, S.-L. Oh, Y.-R. Kim, and K.-H. Yoo, Appl. Phys. Lett. **96**, 023115 (2010); S. Mubeen, G. Hernandez-Sosa, D. Moses, J. Lee, and M. Moskovits, Nano Lett. **11**, 5548 (2011).
[11]S. K. Cushing, J. Li, J. Bright, B. T. Yost, P. Zheng, A. D. Bristow, and N. Wu, J. Phys. Chem. C **119**, 16239 (2015).
[12]Y. Yang, H. B. Gobeze, F. D'Souza, R. Jankowiak, and J. Li, Adv. Mater. Interfaces **3**, 1600371 (2016).
[13]M. Adachi, Y. Murata, J. Takao, J. Jiu, M. Sakamoto, and F. Wang, J. Am. Chem. Soc. **126**, 14943 (2004).
[14]W. Li and D. Zhao, Adv. Mater. **25**, 142 (2013).
[15]Z. Li, C. Rochford, F. J. Baca, J. Liu, J. Li, and J. Wu, Nanoscale Res. Lett. **5**, 1480 (2010).
[16]C. Rochford, Z.-Z. Li, J. Baca, J. Liu, J. Li, and J. Wu, Appl. Phys. Lett. **97**, 043102 (2010).
[17]V. Subramanian, E. E. Wolf, and P. V. Kamat, J. Am. Chem. Soc. **126**, 4943 (2004).
[18]W. Göpel, G. Rocker, and R. Feierabend, Phys. Rev. B **28**, 3427 (1983).
[19]Y. Zheng, S. Klankowski, Y. Yang, and J. Li, ACS Appl. Mater. Interfaces **6**, 10679 (2014).